Self-Passivation of Defects: Effects of High-Energy Particle Irradiation on the Elastic Modulus of Multilayer Graphene

Kai Liu, Cheng-Lun Hsin, Deyi Fu, Joonki Suh, Sefaattin Tongay, Michelle Chen, Yinghui Sun, Aiming Yan, Joonsuk Park, Kin M. Yu, Wenli Guo, Alex Zettl, Haimei Zheng, Daryl C. Chrzan, and Junqiao Wu*

Self-healing materials that can repair damage related to defects or cracks have attracted increasing attentions in recent years. However, they are mostly limited to polymers. Self-healing defects in graphene open up an interesting possibility.[1] As one of the strongest materials, graphene consists of planar sp^2-hybridized carbon bonds.[2–4] It has an extremely high 2D modulus of 340 N m^{-1} and an ultimate tensile strength reaching 42 N m^{-1} (corresponding to Young's modulus of 1 TPa and intrinsic strength of 130 GPa).[3] These excellent mechanical properties make graphene an attractive structural material in applications ranging from people's daily life to space exploration.[5–8] However, applications of graphene in some

Prof. K. Liu, Prof. C.-L. Hsin, Dr. D. Fu,
J. Suh, Dr. S. Tongay, M. Chen,
Prof. D. C. Chrzan, Prof. J. Wu
Department of Materials Science and Engineering
University of California
Berkeley, CA 94706, USA
E-mail: wuj@berkeley.edu
Prof. K. Liu
School of Materials Science and Engineering
Tsinghua University
Beijing 100084, China
Prof. C.-L. Hsin
Department of Electrical Engineering
National Central University
Tao Yuan 32001, Taiwan
Dr. Y. Sun, Dr. A. Yan, Prof. A. Zettl
Department of Physics
University of California
Berkeley, CA 94720, USA
Dr. A. Yan, Dr. K. M. Yu, Prof. A. Zettl, Dr. H. Zheng
Materials Science Division
Lawrence Berkeley National Laboratory
Berkeley, CA 94706, USA
Dr. A. Yan, Prof. A. Zettl
Kavli Energy NanoSciences Institute at the University of California
Berkeley and the Lawrence Berkeley National Laboratory
Berkeley, CA 94720, USA
J. Park
Department of Material Science and Engineering
Stanford University
Stanford, CA 94305, USA
Prof. W. Guo
Department of Physics
City University of New York/QCC
Bayside, NY 11364, USA

extreme conditions, such as those with high-energy irradiation in outer space, result in various crystal defects that weaken this intrinsically strong material.[9] For example, in the outer space, the energy of cosmic rays, which mainly consist of protons and He^{2+} particles, is extremely high. Their energy distribution peaks at ≈0.3 GeV and the corresponding flux is about 1 ions cm^{-2} s^{-1}. The irradiation dose accumulates with exposure time in the outer space. Graphene's resistance to high-energy radiation damage and whether it can heal itself within such an environment remain to be understood.

Graphene flakes exfoliated from high-quality graphite are nearly devoid of high-density defects. Typically, they demonstrate ultrahigh elastic modulus and strength that are close to theoretical values.[3] Unlike exfoliated graphene flakes, however, large-area graphene grown by chemical vapor deposition (CVD) is polycrystalline. It usually contains a large number of localized and extended defects that degrade its physical properties.[10–14] The Young's modulus and tensile strength of CVD graphene were reported to be significantly weaker than exfoliated ones.[15,16] However, with careful post-growth processing used to avoid damages and rippling, these values become very close to exfoliated ones despite the existence of grain boundaries.[17] Theoretical studies predict that grain boundaries formed by five to seven carbon rings enhance or degrade the mechanical properties depending on the angle and geometry of such boundaries,[18,19] but a high density of isolated point defects tend to degrade these properties. On the other hand, although vacancy defects are known to have significant influence on electronic properties of graphene,[20] their effects on mechanical properties are not well investigated experimentally. High-energy (≈MeV) light particle radiation usually creates localized defects on demand and penetrates deep (>μm) into the sample, providing a way to probe atomic-scale defects in graphene. This is in sharp contrast to low-energy oxygen or argon plasma techniques in generating defects in graphene for mechanical studies,[21,22] which may not penetrate deep into multilayer graphene.

In this work, we study the behavior of elastic modulus of exfoliated monolayer, bilayer, and multilayer graphene flakes as a function of localized defects produced by irradiation with high-energy He^{2+} ions (α particles). The modulus is insensitive to these defects until a threshold defect density, after which the modulus decreases rapidly. Interestingly, above the threshold, the rate of degradation in the elastic modulus is the highest for monolayers; it becomes lower for multilayer graphene as the number of layers goes up. Molecular dynamics simulations

**ADVANCED
MATERIALS**

www.advmat.de

Materials
Views

www.MaterialsViews.com

COMMUNICATION

show that irradiation of multilayer graphene creates interlayer linking that has the potential to passivate the defects inside layers. The elastic modulus of multilayers shows enhanced resistance to radiation damage as compared to monolayers. Our findings reveal the importance of interlayer linking from the mechanical perspective, thus shedding light on possibility of engineering graphene properties with controlled defects.

Figure 1a shows a schematic of a graphene flake transferred on holey substrates and irradiated by 3 MeV He^{2+} ions. Their 2D elastic modulus (E^{2D}) is measured by indenting the center of these circular, free-standing graphene membranes with an atomic force microscope (AFM) tip (Figure 1b). Examples of exfoliated monolayer, bilayer, and pentalayer graphene flakes on the holey substrate are shown in Figure 1c,d. The

number of layers of each flake was confirmed by its Raman spectrum and the thickness measured by AFM. Raman spectroscopy is a fast, reliable, and non-destructive technique to identify the number of graphene layers as well as their defect density levels.[23–26] As shown in Figure 1e, the sharp G peak at ≈1580 cm^{-1} associated with the doubly degenerate zone-center E_{2g} mode[23,25] slightly red-shifts as the number of layers increases. Monolayer flake shows a single, sharp, and intense 2D peak at 2680 cm^{-1}, nearly two times stronger than the G peak, corresponding to the second order of zone-boundary phonons.[23] For bilayer and pentalayer flakes, however, the 2D peak is broadened, split, blue-shifted, and significantly reduced in intensity. The D peak expected at ≈1350 cm^{-1}, which is the defect-activated breathing mode of six-atom rings, is not observed in these pristine flakes, proving the high quality of the graphene free of detectable defects. These Raman features are consistent with previous reports.[23,25]

The AFM topography of a monolayer flake covering tens of holes is shown in **Figure 2**a. The enlarged image reveals that these free-standing membranes are taut over the holes, and free of ripples or wrinkles (Figure 2b and Figure S1, Supporting Information). This rules out the effect of ripples that may result in apparently softened modulus of graphene.[15] The indentation tip is pointed at the center of the holes covered with graphene. Three typical force–displacement curves for monolayer, bilayer, and pentalayer graphene membranes are shown in Figure 2c. Such a force–displacement behavior can be described by the following equation:[3,17]

$$F = (\sigma^{2D}\pi)\delta + \left(E^{2D}\frac{q^3}{r^2} \right)\delta^3 \qquad (1)$$

where F is the applied point force, δ is the indentation depth at the center of the membrane, r is the radius of the hole, σ^{2D} is the pretension of the membrane, E^{2D} is the 2D elastic modulus, and q is a constant related to Poisson's ratio (ν) of the membrane, following $q = 1/(1.05 - 0.15\nu - 0.16\nu^2)$. We take $\nu = 0.165$, such that $q = 0.98$.[27] As shown in Figure 2b, Equation (1) fits very well with the experimental curves of all three flakes, from which σ^{2D} and E^{2D} can be derived.

Figure 2d shows that obtained values of E^{2D} are well described by the Gaussian distribution. The average E^{2D} values of monolayer, bilayer, and pentalayer are 355 ± 11, 697 ± 31, and 1736 ± 62 N m^{-1}, respectively. These E^{2D} values behave linearly as a function of the number of layers (inset of Figure 2c), implying that the interlayer van der Waals interaction in graphene is sufficiently strong, such that no interlayer shearing occurs
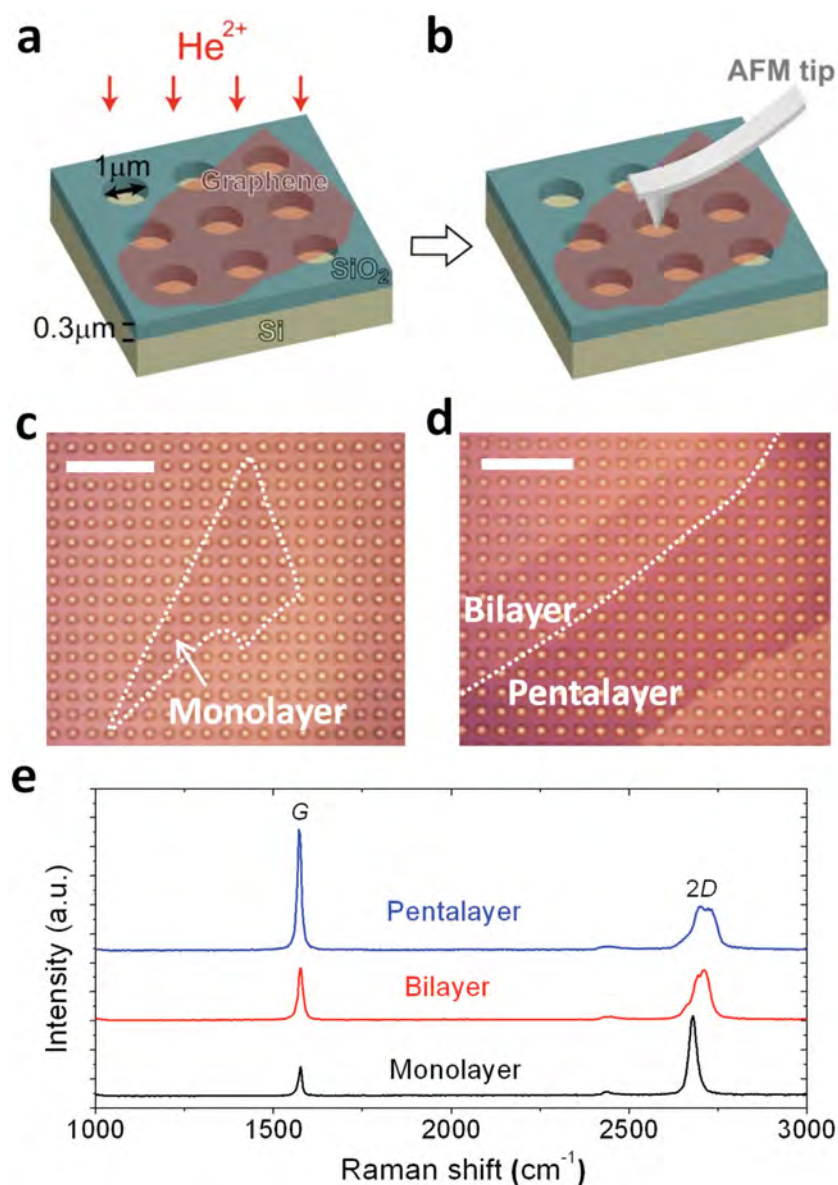

Figure 1. a,b) Schematic of the experiments. c) Optical images of an exfoliated graphene monolayer flake, and d) bilayer and pentalayer flakes on holey substrates. Scale bars, 10 μm. e) Raman spectra of the three pristine graphene flakes.
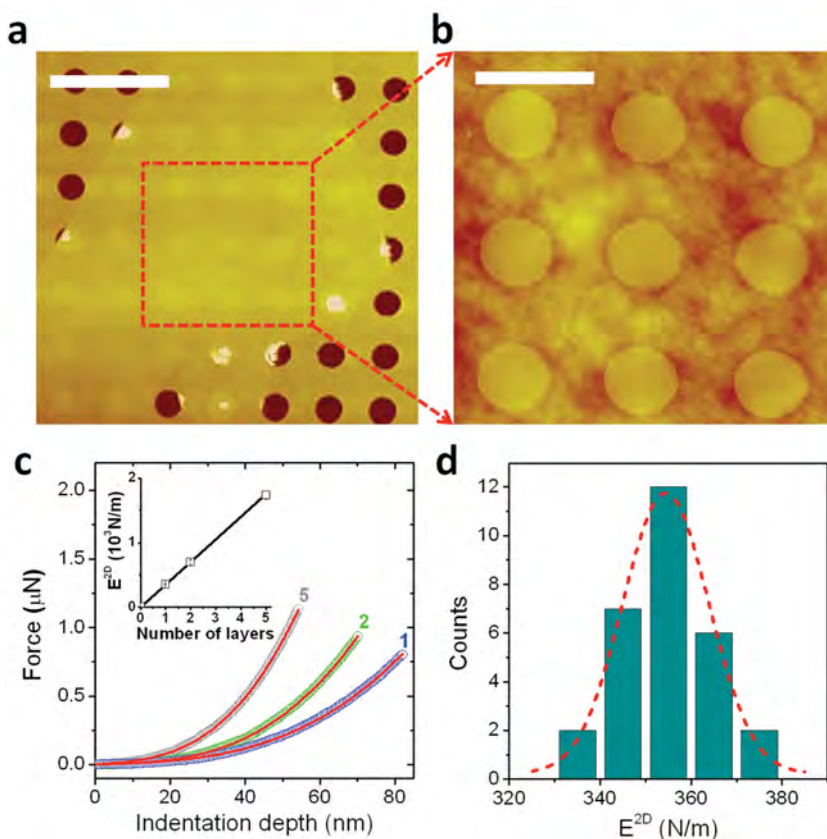
Materials
Views
www.MaterialsViews.com

ADVANCED
MATERIALS
www.advmat.de

Figure 2. a) Tapping-mode AFM image of a monolayer flake on the holey substrate. Scale bar, 5 µm. b) Enlarged AFM image showing taut, free-standing membranes over holes. Scale bar, 2 µm. c) Force–displacement curve of the three pristine graphene flakes. Lines are least-square fitting following Equation (1). The inset shows the measured E^{2D} as a function of the number of layers. d) Statistical histogram of the measured E^{2D} of the monolayer flake over various holes. Dashed line is a fit with the Gaussian distribution.

Supporting Information). Figure 3c plots normalized E^{2D} as a function of cumulative irradiation dose ranging from 4×10^{12} to 1×10^{15} ions cm^{-2}. Based on the behavior of E^{2D}, the range of dose can be divided into three regimes: low doses (<10^{13} ions cm^{-2}), medium doses (10^{13} to 3×10^{14} ions cm^{-2}), and high doses (>3×10^{14} ions cm^{-2}).

In the low-dose regime, E^{2D} remains nearly a constant, insensitive to the defects. This insensitivity may be responsible for the fact that the modulus and mechanical properties of good-quality CVD graphene are similar to those of exfoliated graphene. It is worthy to note that within the low-dose regime, each graphene membrane has experienced ≈10 times AFM contact mode sweeping. Hence, the constant E^{2D} in this regime confirms that the AFM sweeping with small forces indeed does not damage or weaken the graphene.

When the dose is higher than 10^{13} ions cm^{-2}, E^{2D} starts to decrease, as the high density of point defects weakens the average atomic bonds in the graphene. In contrast, the measured values of pretension fluctuate and do not show a clear trend over the range of irradiation dose, revealing that the irradiation does not loosen the membrane that could result in the modulus softening (Figure S5, Supporting Information). However, the E^{2D} curves show a clear dip at the dose of 3×10^{14} ions cm^{-2}. After that (in the high-dose regime) E^{2D} begins to increase. We attribute the abnormal increase in E^{2D} at doses higher than 3×10^{14} ions cm^{-2} to the effect of residual contamination layer. Under such high doses, the contamination layer tends to form a continuous film and becomes difficult to be thoroughly cleaned. After the AFM sweeping, the remaining amount of contamination may be different for the samples with different number of layers (Figure S3, Supporting Information). Therefore, we do not perform quantitative analysis of the abnormal increase in E^{2D}.

It would be interesting to correlate the decrease in modulus to the density of irradiation-induced defects. Experimentally, the ratio of the D and G peak intensities in Raman spectrum was used to estimate the defect density in graphene.[24,26] Because the D peak results from the first-order scattering activated by disorder due to the finite crystallite size, this ratio is related to an average, characteristic crystal size, L_D, following the equation $L_D^2 = C\lambda_L^4 I_G / I_D$, where C is a constant and λ_L is the laser wavelength. It has been correlated to the density of point-like defects generated under low-energy irradiation at low doses.[26] However, MeV irradiation may create defects with relatively large sizes due to multiple-step collisions of high energy ions and secondary atoms, making it difficult to estimate the defect density directly from the Raman spectrum. On the other hand, a simulation of the nanoindentation on vacancies-containing
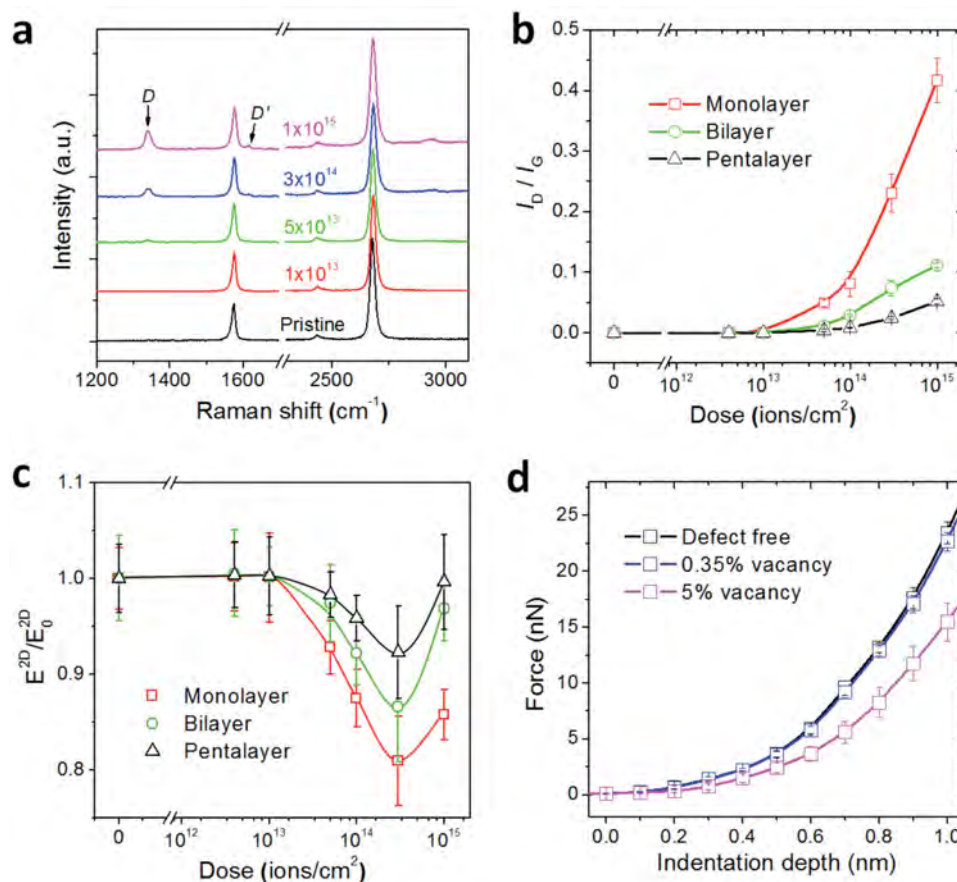
during the AFM indentation measurements. This is very different from the behavior of layered MoS$_2$.[28,29]

The defects introduced by the ion irradiation in graphene can be characterized by Raman spectroscopy.[24,26] As shown in **Figure 3**a, the D peak at ≈1350 cm^{-1}, originating from the intervalley (K–K′) one-phonon double-resonance process, appears at the dose of 5×10^{13} ions cm^{-2}. As the irradiation dose increases, the number of defect sites increases. In this case, Bloch states are mixed around the K (and K′) symmetry points, therefore, Raman selection rules are relaxed and the D peak is enhanced (Figure 3b). Double resonance also occurs in the intravalley process, resulting in a D peak at 1620 cm^{-1} (Figure 3a), which is very close to the strong G peak and typically unnoticeable in graphene with low densities of defects. However, both the G and 2D peaks remain sharp and intense after irradiation, indicating that the sp^2 bond character is still preserved in the graphene, and amorphization does not occur.[24,26]

In order to reliably probe the effect of irradiation on the graphene modulus, the same group of membrane holes was used, and the irradiation was carried out sequentially followed by measurements at each accumulative doses. A thin contamination layer appeared after high-dose irradiation and was carefully removed to avoid its effect on the measurements (see Figure S2–S4,

Figure 3. a) Raman spectra of monolayer graphene after various doses of ion irradiation. b) Intensity ratio of the D and G peaks (I_D/I_G) of the three flakes as a function of irradiation dose. The difference of I_D/I_G for flakes with different number of layers may result from different scaling rules between I_D/I_G and defect density, owing to different band structures. c) Normalized E^{2D} of the three flakes as a function of irradiation dose. d) Simulated force curves of indentation processes under different defect densities. The simulation is carried out on pretension-free membranes, and the modulus can be derived by fitting the curves with the cubic term in Equation (1).

monolayer graphene shows that the load force drops with increased vacancy density, reducing the modulus by ≈3% at 0.35% vacancy, and by ≈40% at 5% vacancy (Figure 3d). Compared to Figure 3c, this result suggests that the density of defects in monolayer graphene created by 3×10^{14} ions cm^{-2} irradiation is on the order of 1%.

It is interesting to point out that in the medium-dose regime, the elastic modulus of graphene with more layers degrades less (Figure 3c). This is not a straightforward result, because to the first-order approximation, the areal defect density per layer should be the same regardless of the total number of layers in the graphene flake. The projected range is ≈9 μm in graphitic materials when 3 MeV He^{2+} is used. Therefore, to a good approximation, an N-layer graphene is expected to be equivalent to N graphene monolayers independently stacked together, and the measured E^{2D} normalized by N should behave exactly the same (as it does in pristine samples) as a function of irradiation dose, independent from N. The mechanical strengthening by a possible residual contamination deposition can also be excluded. In this range of medium doses, the carbon residues are particles-like (Figure S2, Supporting Information) and easy to remove. After the AFM sweeping, the carbon residues on the

surface, if any, should have negligible effect on the measured 2D moduli.

Interlayer shearing may also reduce the effective modulus of multilayer materials, as shown in bilayer 2D semiconductors.[28,29] Whether interlayer shearing occurs depends on the type of layered material and the applied strain. In this work, we indent graphene layers to a small depth (50–80 nm, as shown in Figure 2c), corresponding to a small strain of only ≈1%. The measured E^{2D} in this case depends linearly on the number of graphene layers (Figure 2c), and the linearity holds with increasing irradiation dose up to 10^{13} ions cm^{-2}, after which the measured modulus begins to drop. Therefore, the interlayer shearing does not occur at the dose <10^{13} ions cm^{-2}. At irradiation doses >10^{13} ions cm^{-2}, if there was an interlayer shearing, it would reduce the effective 2D modulus of multilayer graphene, leading to a lower normalized modulus of multilayer graphene compared to monolayer graphene, which is the opposite to our observation (Figure 3c). Therefore, we can rule out the possibility that interlayer shearing plays an important role in the measurements.

The stronger robustness against irradiation in multilayers than monolayers suggests a defect self-healing mechanism in
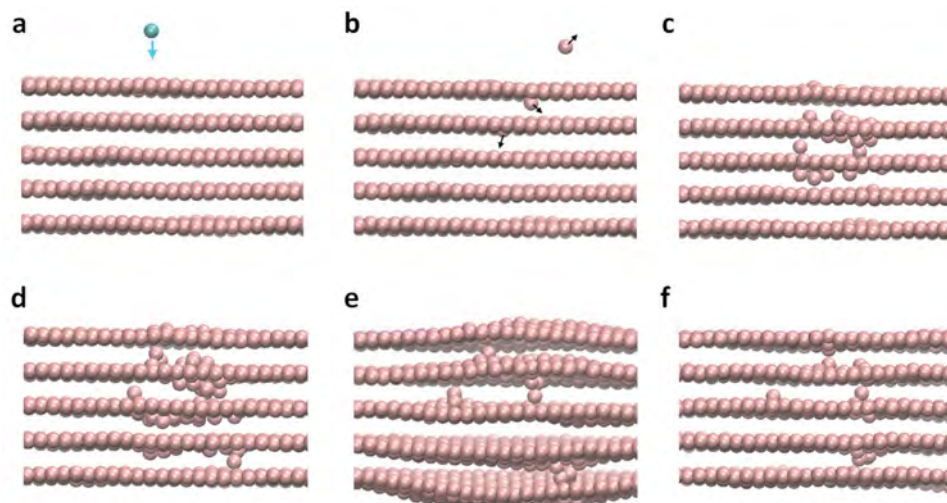
Materials
Views
www.MaterialsViews.com

ADVANCED
MATERIALS
www.advmat.de

Figure 4. A series of time-sequential images (a–f) clipped from the simulation, showing the He^{2+} irradiation and the formation of interlayer linking in a five-layer graphene. The cyan sphere is the He^{2+} particle and light-brown spheres represent carbon atoms. The elapsed time after He^{2+} penetration is about: 3 attosecond (as) (b), 9 as (c), 14 as (d), 138 as (e), and 1 femtosecond (fs) (f).

multilayers. It was reported that defective graphene can partially self-heal by thermal annealing in which the defect sites trap mobile carbon atoms.[1] This healing process may also happen in the multilayer graphene under ion irradiation,[30] where carbon atoms bombarded out of one layer can be captured by defect sites on another layer or between layers. The former may heal the defect sites, while the latter may form interlayer links across defect sites. Both activities would in situ heal the multilayer graphene during the radiation process. Graphene with more layers has a smaller surface-to-volume ratio, thus it has a higher chance for this to occur, behaving more robust against radiation damage.

High-energy He^{2+} irradiation was simulated by the molecular dynamics (MD) method in order to investigate these two actions in the multilayer graphene. In the simulation, we have observed the formation of mono vacancies, di-vacancies, and larger vacancy clusters, as well as the formation of the Stone–Wales defects, and defects that crosslink the layers. This range of defects is possible because the kinetic energy of the He ions, 3 MeV, can break many C–C bonds in the graphene layer. A typical formation process of defects generated by the irradiation of a 3 MeV He^{2+} ion is shown in **Figure 4**. The He^{2+} ion flies through the graphene layers very quickly, depositing a short and intense force impulse to impinged carbon atoms. Several carbon atoms are scattered out after the collision (Figure 4a,b), creating different types of defects in the graphene layers. The carbon atoms back-scattered from the surface layer escape the graphene (Figure 4b). However, those carbon atoms moving inward might interact with other carbon atoms in the layers and can be eventually trapped between layers (Figure 4c,d). The collisions caused by He^{2+} and scattered carbon atoms lead to a pulse of wave in the graphene layers and a cascade of damages (Figure 4e). This wave will eventually be damped and relaxed via thermal fluctuation, forming interlayer links (Figure 4f). A typical link includes an interlayer sp^3 bonding as well as a distorted lattice, which emerges out of one layer but interacts with

adjacent layers. The interlayer links that occur mostly around the localized defects caused by irradiation would partially compensate the defects-induced weakening of the modulus, effectively passivating the defects inside the layer. Our simulation also shows that there is a significant possibility of creating a dramatically large area of vacancy defects under such high-energy irradiations, either for monolayer graphene or multilayers, which supports our discussion on the estimation of defect density.

Some theoretical efforts reported decrease of elastic modulus of monolayer graphene with increase in the density of defects.[31,32] Experimentally, Zandiatashbar et al. studied the effect of oxygen plasma-induced defects, which include several types of defects and even large voids, on the mechanical properties of monolayer graphene.[21] In this case, the elastic modulus remains unchanged until a high density of vacancy defects. López-Polín et al., however, reported a different result, where the elastic modulus dramatically increases at initial, low density of mono vacancies introduced by low-energy Ar$^+$ irradiation.[22] The initial increase was attributed to dependence of the elastic coefficients on the momentum of flexural modes for 2D membranes within the framework of thermodynamic theory. This effect, however, would be hidden by existence of various types of defects and large-area vacancies that can significantly reduce the elastic modulus in oxygen plasma etching. As our MD simulation shows formation of various types of defects and large vacancy clusters, the effect of high-energy He^{2+} irradiation is more like that of oxygen plasma, rather than that of low-energy Ar$^+$ irradiation. This may explain our observation of unchanged elastic modulus at low doses of irradiation, consistent with that of Zandiatashbar et al.[21]

There are likely implications of our work to structural applications of graphene-like materials. The interlayer links between graphene layers have the potential to improve mechanical properties of graphene-like materials in a number of ways. First, the interlayer links will prevent the sliding of

COMMUNICATION

layers relative to one another, and this might increase the bending modulus of the layers. Second, the links between graphene layers will enable load distribution between the layers.[33] This might serve to blunt or halt the propagation of cracks, and thereby increase the toughness of multilayered materials. Third, the interlayer links will serve to pin the thermal ripples of individual layers. This pinning, then, might influence the effective elastic moduli for the graphene layers.[22] All of these effects leave interesting topics for future work both in experiments and calculations.

In summary, we investigated the thickness dependence of the weakening of graphene modulus under high-energy He^{2+} particle irradiation. Our results suggest that monolayer graphene is more sensitive to the high-energy irradiation damage compared to multilayer graphene. In multilayer graphene, the scattered carbon atoms can be trapped between layers and tend to form interlayer linking around the defects to partially restore the degraded modulus. These findings reveal the importance of interlayer linking from the mechanical perspective, thus shed light for possibly engineering graphene properties with controlled defects. Our results may be also applicable to other layered materials, such as 2D transition metal dichalcogenides and their heterostructures.

Experimental Section

Graphene Transfer and Nanoindentation: Graphene thin flakes (monolayer, bilayer, and pentalayer) used in this study were exfoliated on holey substrates from bulk graphite flakes (NGS Naturgraphit GmbH). Each flake was larger than 10 μm in size and covered more than 20 holes. The holey substrates were prepared by deep-UV photolithography followed by a deep reactive ion etching of a SiO$_2$/Si wafer. The size of the circular holes was 1 μm in diameter and 0.3 μm in depth. Graphene flakes on holey substrates were then irradiated by 3 MeV He^{2+} ions with a uniform spot size of ≈6 mm under a vacuum with a pressure of ≈4 × 10^{-6} Torr. To measure elastic moduli of graphene flakes, an AFM (Bruker Multimode) tip (μmash, HQ: NSC15, diamond-like carbon coated, tip diameter ≈20 nm) was used to indent the center of the circular, free-standing graphene membranes. The spring constant of the tip was calibrated by a reference cantilever. Six to nine holes were selected for each type of graphene flakes, and three to four force–displacement curves on each hole were measured by applying various maximum forces (0.4–1.5 μN). In total, 18–30 values of σ^{2D} and E^{2D} for each type of flakes were independently acquired.

Molecular Dynamic Simulation: The simulations employ LAMMPS.[34] The graphene layers were modeled using the ARIEBO potential in ref. [35] The He ion/graphene interaction was modeled using the ZBL potential.[36] Periodic boundary conditions were employed in the plane of the graphene sheet. The samples were first equilibrated at room temperature using an NPT ensemble with zero pressure, which allowed the expected thermal ripples to form. The high energy He^{2+} ion was then introduced into the simulation and the timestep was set to very short time ≈1.5 × 10^{-8} ps, and the simulation ran under NVE conditions for 10 000 timesteps. The timestep was then increased to ≈9.2 × 10^{-8} ps and an additional 10 000 timesteps were run within an NPT ensemble. The timestep was further increased to 5 × 10^{-5} ps, and the sample relaxed under NPT conditions. Atoms scattered away from the graphene were removed from the simulation. Since our intent was to study the effects of a successful collision, we "aimed" the ion at a C atom in the graphene sheet chosen at random. Our "aim" was chosen to be imperfect, and a wide range of collision results ranging from no interaction to extreme damage were obtained. Though we did not have information concerning the relative frequencies of these differing events, the simulations did

provide insight into the types of damage that could occur during the He^{2+} scattering.

Simulation of Nanoindentation: The simulation was carried out on a free-standing circular monolayer graphene membrane. The membrane was initially set to be free of pretension and have randomly distributed vacancies with different densities. After simulated equilibration at room temperature, the atoms on the edge of the membrane were fixed, and the indentation simulation was conducted. The diameter of the membrane was 7.5 nm, and the diameter of the indenter was 2 nm. The errors estimated in the applied force were obtained by averaging over either 16 or 32 independent simulations. An indentation depth of 0.7 nm generated a similar strain of graphene membrane in this simulation as the maximum value in the experimental indentation. The elastic modulus was derived by fitting a force curve with the cubic term in Equation (1), as the linear term was not considered here due to lack of pretension.

Supporting Information

Supporting Information is available from the Wiley Online Library or from the author.

Acknowledgements

[1] J. Chen, T. Shi, T. Cai, T. Xu, L. Sun, X. Wu, D. Yu, *Appl. Phys. Lett.* **2013**, *102*, 103107.

[2] K. S. Novoselov, D. Jiang, F. Schedin, T. J. Booth, V. V. Khotkevich, S. V. Morozov, A. K. Geim, *Proc. Natl. Acad. Sci. USA* **2005**, *102*, 10451.

[3] C. Lee, X. Wei, J. W. Kysar, J. Hone, *Science* **2008**, *321*, 385.

[4] K. S. Novoselov, V. I. Fal'ko, L. Colombo, P. R. Gellert, M. G. Schwab, K. Kim, *Nature* **2012**, *490*, 192.

[5] T. Ramanathan, A. A. Abdala, S. Stankovich, D. A. Dikin, M. Herrera-Alonso, R. D. Piner, D. H. Adamson, H. C. Schniepp, X. Chen, R. S. Ruoff, S. T. Nguyen, I. A. Aksay, R. K. Prud'Homme, L. C. Brinson, *Nat. Nanotechnol.* **2008**, *3*, 327.

[6] S. Stankovich, D. A. Dikin, G. H. Dommett, K. M. Kohlhaas, E. J. Zimney, E. A. Stach, R. D. Piner, S. T. Nguyen, R. S. Ruoff, *Nature* **2006**, *442*, 282.

[7] Z. Xu, C. Gao, *Nat. Commun.* **2011**, *2*, 571.

[8] Y. Kim, J. Lee, M. S. Yeom, J. W. Shin, H. Kim, Y. Cui, J. W. Kysar, J. Hone, Y. Jung, S. Jeon, S. M. Han, *Nat. Commun.* **2013**, *4*, 2114.

[9] A. A. Griffith, *Philos. Trans. R. Soc. London Ser. A* **1921**, *221*, 163.

[10] A. Reina, X. Jia, J. Ho, D. Nezich, H. Son, V. Bulovic, M. S. Dresselhaus, J. Kong, *Nano Lett.* **2009**, *9*, 30.

[11] X. Li, W. Cai, J. An, S. Kim, J. Nah, D. Yang, R. Piner, A. Velamakanni, I. Jung, E. Tutuc, S. K. Banerjee, L. Colombo, R. S. Ruoff, *Science* **2009**, *324*, 1312.

[12] Z. Sun, Z. Yan, J. Yao, E. Beitler, Y. Zhu, J. M. Tour, *Nature* **2010**, *468*, 549.

[13] X. Li, C. W. Magnuson, A. Venugopal, J. An, J. W. Suk, B. Han, M. Borysiak, W. Cai, A. Velamakanni, Y. Zhu, L. Fu, E. M. Vogel, E. Voelkl, L. Colombo, R. S. Ruoff, *Nano Lett.* **2010**, *10*, 4328.

[14] P. Y. Huang, C. S. Ruiz-Vargas, A. M. van der Zande, W. S. Whitney, M. P. Levendorf, J. W. Kevek, S. Garg, J. S. Alden, C. J. Hustedt, Y. Zhu, J. Park, P. L. McEuen, D. A. Muller, *Nature* **2011**, *469*, 389.

[15] C. S. Ruiz-Vargas, H. L. Zhuang, P. Y. Huang, A. M. van der Zande, S. Garg, P. L. McEuen, D. A. Muller, R. G. Hennig, J. Park, *Nano Lett.* **2011**, *11*, 2259.

[16] Q.-Y. Lin, G. Jing, Y.-B. Zhou, Y.-F. Wang, J. Meng, Y.-Q. Bie, D. P. Yu, Z.-M. Liao, *ACS Nano* **2013**, *7*, 1171.

[17] G. H. Lee, R. C. Cooper, S. J. An, S. Lee, A. van der Zande, N. Petrone, A. G. Hammerberg, C. Lee, B. Crawford, W. Oliver, J. W. Kysar, J. Hone, *Science* **2013**, *340*, 1073.

[18] R. Grantab, V. B. Shenoy, R. S. Ruoff, *Science* **2010**, *330*, 946.

[19] Y. Wei, J. Wu, H. Yin, X. Shi, R. Yang, M. Dresselhaus, *Nat. Mater.* **2012**, *11*, 759.

[20] S. Nakaharai, S. Iijima, S. Ogawa, S. Suzuki, S.-L. Li, K. Tsukagoshi, S. Sato, N. Yokoyama, *ACS Nano* **2013**, *7*, 5694.

[21] A. Zandiatashbar, G.-H. Lee, S. J. An, S. Lee, N. Mathew, M. Terrones, T. Hayashi, C. R. Picu, J. Hone, N. Koratkar, *Nat. Commun.* **2014**, *5*, 3186.

[22] G. López-Polín, C. Gómez-Navarro, V. Parente, F. Guinea, M. I. Katsnelson, F. Pérez-Murano, J. Gómez-Herrero, *Nat. Phys.* **2014**, *11*, 26.

[23] A. C. Ferrari, J. C. Meyer, V. Scardaci, C. Casiraghi, M. Lazzeri, F. Mauri, S. Piscanec, D. Jiang, K. S. Novoselov, S. Roth, A. K. Geim, *Phys. Rev. Lett.* **2006**, *97*, 187401.

[24] M. M. Lucchese, F. Stavale, E. H. M. Ferreira, C. Vilani, M. V. O. Moutinho, R. B. Capaz, C. A. Achete, A. Jorio, *Carbon* **2010**, *48*, 1592.

[25] E. H. Martins Ferreira, M. V. O. Moutinho, F. Stavale, M. M. Lucchese, R. B. Capaz, C. A. Achete, A. Jorio, *Phys. Rev. B* **2010**, *82*, 125429.

[26] L. G. Cancado, A. Jorio, E. H. Ferreira, F. Stavale, C. A. Achete, R. B. Capaz, M. V. Moutinho, A. Lombardo, T. S. Kulmala, A. C. Ferrari, *Nano Lett.* **2011**, *11*, 3190.

[27] O. L. Blakslee, *J. Appl. Phys.* **1970**, *41*, 3373.

[28] S. Bertolazzi, J. Brivio, A. Kis, *ACS Nano* **2011**, *5*, 9703.

[29] K. Liu, Q. Yan, M. Chen, W. Fan, Y. Sun, J. Suh, D. Fu, S. Lee, J. Zhou, S. Tongay, J. Ji, J. B. Neaton, J. Wu, *Nano Lett.* **2014**, *14*, 5097.

[30] M. Kalbac, O. Lehtinen, A. V. Krasheninnikov, J. Keinonen, *Adv. Mater.* **2013**, *25*, 1004.

[31] R. Dettori, E. Cadelano, L. Colombo, *J. Phys.: Condens. Matter* **2012**, *24*, 104020.

[32] N. Jing, Q. Xue, C. Ling, M. Shan, T. Zhang, X. Zhou, Z. Jiao, *RSC Adv.* **2012**, *2*, 9124.

[33] B. Peng, M. Locascio, P. Zapol, S. Li, S. L. Mielke, G. C. Schatz, H. D. Espinosa, *Nat. Nanotechnol.* **2008**, *3*, 626.

[34] S. Plimpton, *J. Comput. Phys.* **1995**, *117*, 19.

[35] S. J. Stuart, A. B. Tutein, J. A. Harrison, *J. Chem. Phys.* **2000**, *112*, 6472.

[36] J. F. Ziegler, J. P. Biersack, U. Littmark, *The Stopping and Range of Ions in Solids*, Vol. *1*, Pergamon Press, New York **1985**.